Experimental investigation of terahertz quantum cascade laser with variable barrier heights

Aiting Jiang, Alpar Matyas, Karun Vijayraghavan, Christian Jirauschek, Zbig R. Wasilewski, and Mikhail A. Belkin

Citation: Journal of Applied Physics **115**, 163103 (2014); doi: 10.1063/1.4873461
View online: http://dx.doi.org/10.1063/1.4873461
View Table of Contents: http://scitation.aip.org/content/aip/journal/jap/115/16?ver=pdfcov
Published by the AIP Publishing

Experimental investigation of terahertz quantum cascade laser with variable barrier heights

Aiting Jiang,[1] Alpar Matyas,[2] Karun Vijayraghavan,[1] Christian Jirauschek,[2]
Zbig R. Wasilewski,[3] and Mikhail A. Belkin[1,a)]
[1]*Department of Electrical and Computer Engineering, The University of Texas at Austin, Austin, Texas 78758, USA*
[2]*Institute for Nanoelectronics, Technische Universität München, D-80333 Munich, Germany*
[3]*Department of Electrical and Computer Engineering, University of Waterloo, Waterloo, Ontario N2L 3G, Canada*

(Received 15 March 2014; accepted 14 April 2014; published online 23 April 2014)

We report an experimental study of terahertz quantum cascade lasers with variable barrier heights based on the $Al_xGa_{1-x}As/GaAs$ material system. Two new designs are developed based on semiclassical ensemble Monte Carlo simulations using state-of-the-art $Al_{0.15}Ga_{0.85}As/GaAs$ three-quantum-well resonant phonon depopulation active region design as a reference. The new designs achieved maximum lasing temperatures of 188 K and 172 K, as compared to the maximum lasing temperature of 191 K for the reference structure. These results demonstrate that terahertz quantum cascade laser designs with variable barrier heights provide a viable alternative to the traditional active region designs with fixed barrier composition. Additional design space offered by using variable barriers may lead to future improvements in the terahertz quantum cascade laser performance. © *2014 AIP Publishing LLC*. [http://dx.doi.org/10.1063/1.4873461]

I. INTRODUCTION

After a decade of development, the maximum operating temperature (T_{max}) of Terahertz (THz) Quantum Cascade Lasers (QCLs) has been improved from 50 K (Ref. 1) to a current record of 199.5 K.[2] The active region scheme has evolved from chirped superlattice structures[1] to resonant phonon depopulation (RPD) designs[3,4] to obtain higher gain, while the waveguide structure has advanced from plasmon waveguide to copper-copper double metal waveguide[5] to minimize waveguide loss. The best T_{max} so far is based on a three well RPD design and copper-copper waveguide structure.[2] To push T_{max} further towards temperatures accessible by thermoelectric coolers (~240 K) and beyond, more innovations are desired.[6] This paper reports an experimental study on THz active region designs with variable barrier heights as an additional design degree of freedom.

For intersubband laser transitions from the upper laser state u to the lower laser state l, the peak gain g scales as $g \propto \Delta n_{ul} f_{ul}/\Gamma$, where f_{ul} is the oscillator strength, Δn_{ul} is the population inversion, and 2Γ is the full width at half maximum of the transition linewidth. The population inversion Δn_{ul} relies on having a relatively long upper level lifetime τ_u, selective electron injection, and fast extraction. As temperature increases, the transition linewidth broadens, the injection/extraction selectivity degrades, and the lifetime τ_u is significantly reduced by longitudinal optical (LO) phonon scattering of thermal electrons as discussed previously.[7–9] These are main limiting factors for high temperature operation of THz QCLs. Maximizing the oscillator strength f_{ul} appears to be a straightforward way to increase gain. However, as demonstrated in Ref. 10 and clarified in Refs. 2, 11, and 12, there are tradeoffs between f_{ul} and Δn_{ul}, which is referred to as degree of diagonality. Strong overlap of lasing states can increase f_{ul}, but will also increase nonradiative scattering rates and degrade injection selectivity. As a result, simply maximizing f_{ul} will not necessarily improve performance.

Three-well RPD designs based on the GaAs/AlGaAs material system, using 15% aluminum content in the barriers, have shown so far best T_{max} results.[2,5,10] The optimization of f_{ul} and diagonality, as well as electron injection and extraction efficiency is principally performed by adjusting layer thicknesses. The design in Ref. 2 marks the state of the art of such optimization; however, the room for further improvement by changing layer thicknesses is limited. We have recently proposed[13] that varying the barrier heights in the QCL structure may introduce new degree of freedom in a THz QCL design and may help to boost the maximum operating temperature. Since the AlGaAs barriers are lattice matched to the GaAs substrate for effectively any aluminum fraction, AlGaAs/GaAs THz QCLs with variable barrier heights can be easily produced experimentally; however, this design principle has not been used previously with the exception of the report in which a THz QCL design with variable aluminum fraction in wells was demonstrated.[14] We note that introducing aluminum in the THz QCL wells is expected to lead to strong alloy scattering and our designs use GaAs wells throughout the laser structure. In this paper, we present the results of our experimental investigation of two THz QCL designs with variable barrier heights.

II. SIMULATION RESULTS

We started with the 199.5 K structure[2] as a reference and developed two new designs with variable barrier heights. The new designs were optimized based on semiclassical

a)mbelkin@ece.utexas.edu

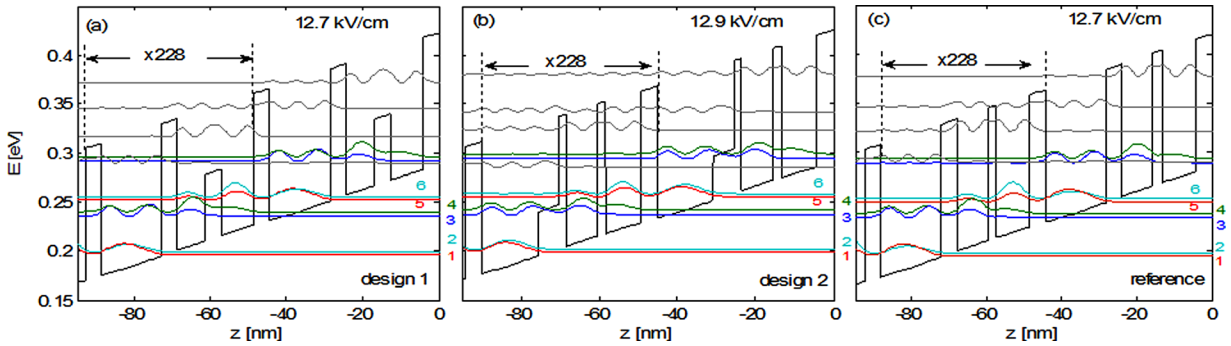

FIG. 1. Conduction band diagram and relevant energy state wavefunctions of the two laser designs: design 1 (a) and design 2 (b), explored experimentally in this report, as well as of the reference structure (c). The structures are shown at the bias voltage of 13.1 kV/cm in (a), 12.9 kV/cm in (b), and 13.2 kV/cm in (c).

ensemble Monte-Carlo (EMC) simulations.[11,13] An attempt was made to introduce only limited structure modifications to be able to make a comparison of performance to the reference structure. The layer sequences of one period of the active regions for the two new designs in Angstrom are (subscripts indicate Al contents in AlGaAs barriers) $43_{0.15}/160_0/41_{0.15}/72_0/46_{0.075}/82_0$ and $43_{0.15}/142_0/54_{0.05}/18_{0.15}/81_0/20_{0.15}/91_0$, where the first and the second structures are referred to as designs 1 and 2, respectively. The simulated conduction band diagrams of two consecutive stages of the structures under applied operating bias voltage are shown in Fig. 1. In the optimization process, the structures have been biased at these voltages and the layers have been changed in order to control the lasing frequency, injection anticrossing, and oscillator strength. Table I is a summary for band diagram information of all three designs at 200 K. Table II is a summary for transport properties of all three designs at 200 K as obtained by EMC under the condition of maximum current density.

For design 1 (Fig. 1(a)), the width of the middle barrier in the lasing double well is increased while the height is reduced. The injection well, barrier, and extraction barrier are kept the same as the reference. Low aluminum-fraction barrier in the active region reduces interface roughness scattering[13] and increases oscillator strength for a laser transition. EMC simulations show an increased oscillator strength ($f_{54,design1} \approx 0.378$) and injection efficiency ($\eta_{5,design1} \approx 50.9\%$, definitions for η_i can be found in Ref. 15) as compared to the reference[2] ($f_{54,reference} \approx 0.293$ and $\eta_{5,reference} \approx 45.6\%$).

For design 2, the extraction barrier is replaced by a step barrier. We adjust the step barrier shape to increase the extraction coupling and decrease the lifetime τ_4 of the lower laser state. The EMC results show an increase of the oscillator strength and injection efficiency to $f_{54,design2} \approx 0.601$ and $\eta_{5,design2} \approx 54.2\%$. The lifetime τ_4 for design 2 has the smallest value among all three designs, showing possible advantage in lower laser state depopulation. We note, however, that the step barrier also introduces parasitic channels that lower the relative depopulation rate r_4/r_0, where $r_0 = J/(e_0 n_{2D})$ is a measure for the overall scattering strength in the structure.

For both design 1 and design 2, a higher simulated current results from an increase of the oscillator strength (Table I) and from parasitic channels (Table II). Overall, EMC simulations indicate that both designs 1 and 2 produce more gain (Fig. 2) compared to the reference structure at high temperatures.

We further note that, by varying the barrier heights, the coupling of the lasing states to the continuum states in the higher minibands can have an adverse influence on the laser gain.[16] Due to the practical limitations of the EMC simulations, these effects have been neglected. Instead, we took a special care to keep the position of higher minibands and energy separation of the lasing states from high miniband states in the new structures to be similar to that in the reference structure.

Fig. 2(a) plots the simulated gain spectra at a lattice temperature of 200 K for all three designs. Both new designs are predicted to have higher peak gain than the reference structure at 200 K. Fig. 2(b) shows the calculated maximum peak gain versus temperature for the two new designs. If we assume a virtual loss of 40 cm^{-1} as in Ref. 13, the expected

TABLE I. Summaary of the oscillator strengths and anticrossings for the three designs at 200 K. $f_{osc} = f^{54}_{osc} + f^{64}_{osc}$ is the total oscillator strength for the laser gain, and f^{54}_{osc} is the main lasing transition oscillator strength. e_{34}, e_{35}, e_{36}, e_{46}, and e_{56} are anticrossing energies (at full alignment) between the level 3, 4, 5, and 6.

	f_{osc}	f^{54}_{osc}	e_{34} (meV)	e_{35} (meV)	e_{36} (meV)	e_{46} (meV)	e_{56} (meV)
Design 1	0.744	0.378	4.8	4.5	1	1.28	2.8
Design 2	0.959	0.601	5.6	5.5	1.1	1.35	2.8
Reference	0.617	0.293	5	4.3	1	1.24	2.8

TABLE II. Comparison of carrier transport parameters for the three designs at 200 K, extracted from EMC simulations at maximum current density. p_4, p_5, and p_6 are the populations for the different levels. η_5 and η_4 are the injection efficiencies into the upper and lower laser levels. J is the maximum current density. r_4/r_0 is the normalized total outscattering rate from level 4 to lower-lying levels, with $r_0^{-1} = e_0 n_{2D}/J$, being the average dwell time of an electron in a period. τ_4 is the lifetime of level 4.

	p_6 (%)	p_5 (%)	p_4 (%)	η_5 (%)	η_4 (%)	J (kA/cm^2)	r_4/r_0	τ_4 (ps)
Design 1	32.3	39.1	15.9	50.9	32.1	1.764	3.87	0.703
Design 2	32.4	36.4	15.5	54.2	27.2	2.099	3.33	0.688
Reference	32.0	40.1	14.5	45.6	30.9	1.674	4.08	0.703

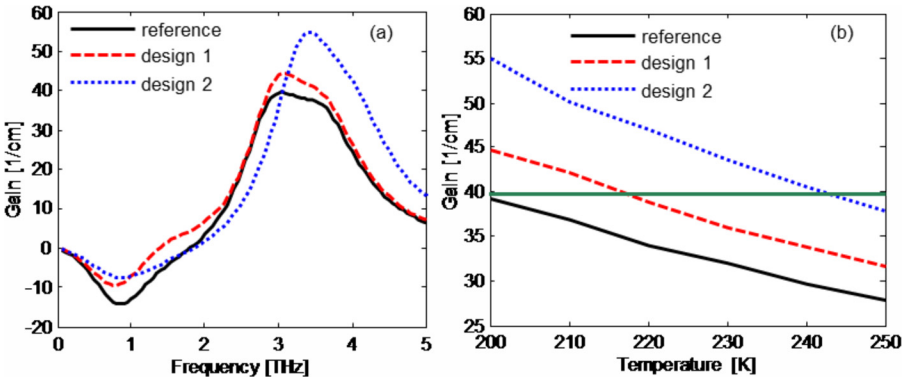

FIG. 2. (a) Gain spectra at a lattice temperature of 200 K calculated using EMC simulations for the reference structure[2] and its two modifications shown in Fig. 1. (b) Peak gain versus temperature calculated for the three structures in (a) using EMC simulations.

T_{max} are approximately 215 K and 240 K for design 1 and design 2, respectively.

III. GROWTH AND PROCESSING

Both design 1 and design 2, together with the 199.5 K reference structure,[2] were grown at the National Research Council of Canada in the V90 VG Semicon Molecular Beam Epitaxy (MBE) system on semi-insulating (001)-oriented GaAs substrates. Arsenic dimers were generated using Veeco Mark V valved cracker source, while two Veeco SUMO cells were used to supply gallium and a dual-filament cell with 40 cc conical crucible was used for aluminum. Both Ga sources were used to grow GaAs at 0.25 nm/s, as well as for the 7.5% or 5% AlGaAs barriers, while only one Ga source was used for the growth of the 15% AlGaAs barriers. To facilitate direct comparison, the same approach was used for the growth of the reference structure. Thus, the growth conditions for the latter were not identical to the original structure which demonstrated T_{max} of 199.5 K, for which only one Ga cell and one Al cell was used for the growth of GaAs at 0.23 nm/s and growth of 15% AlGaAs. Flux drift compensation was employed during the growth.[17] High Resolution X-ray Diffraction measurements revealed that layer thicknesses for all three structures were within 0.5% of the target parameters. The active region thickness was kept at 10 μm. Contact layers structure and QCL active region doping were kept in the same manner as in the 199.5 K reference[2] to ensure the same loss for all structures. More specifically, for all our structures, the injector well is doped to 6×10^{16} cm^{-3} in the middle 50 Å section and the active region is sandwiched between 100 nm of 5×10^{18} cm^{-3} bottom n+ GaAs layer and the top stack of 50 nm of 5×10^{18} cm^{-3} and 10 nm of 4×10^{19} cm^{-3} n+ GaAs layers capped with 3.5 nm LT-GaAs passivation layer.[18]

All three wafers were processed into copper-copper double metal waveguide devices under the same conditions. A metal layer sequence Ta/Cu/Ti/Au (10 nm/350 nm/10 nm/400 nm) was deposited on top of the MBE-grown samples first. Then the chips were flipped and bonded to carriers using Au-Au thermo-compression bonding. After bonding, the sample substrate was selectively removed using $NH_4OH:H_2O_2$ solution. The top n+ contact layer was removed to further reduce the waveguide loss. A metal stack Ta/Cu/Ti/Ni (10 nm/300 nm/10 nm/100 nm) was deposited and patterned through a lift-off process to form 120-μm-wide contacts for the future laser ridges. Cl_2/BCl_3 plasma dry etch was then employed to etch the laser ridges using nickel on top of the ridge contacts as the self-aligned hard mask. The device substrates were then thinned down to ~200 μm, backside metal contact was deposited, and the wafers were cleaved into ~1.5-mm-long laser bars, indium soldered on copper heat sinks, and mounted in a cryostat for measurements.

IV. EXPERIMENTAL RESULTS

Testing was carried out in pulsed mode with 100 ns pulses at a 5 kHz repetition rate. The power was measured with a calibrated helium-cooled Si bolometer. Spectra were measured using a Fourier-transform infrared spectrometer (FTIR).

Output power-current (L-I) characteristics of the devices are presented in Fig. 3. The maximum operating temperatures were measured to be 191 K, 188 K, and 176 K for the

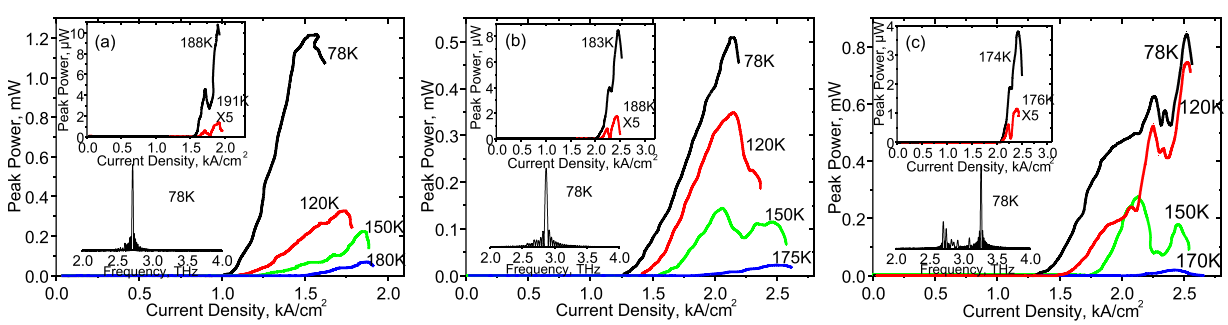

FIG. 3. THz output power vs. current density (L-I) at different heat sink temperatures. THz power data were not corrected for collection efficiency. Insets: L-I characteristics close to T_{max} and lasing spectra at heat sink temperature of 78 K near the maximum power output. Panels (a), (b), and (c) represent results of the reference structure, design 1, and design 2, respectively.

reference, design 1, and design 2 devices, respectively. Design 1 has a T_{max} very close to that of the reference structure, while T_{max} of design 2 degrades considerably, in contrast with EMC predictions. Fig. 4 shows the current-voltage (I-V) characteristics and dV/dI-I characteristics for all structures at 150 K. The dV/dI-I characteristics for the design 1 as well as for the reference structure show a clear differential resistance drop at the beginning of lasing. The relative size of this drop is a measure of the difference of upper and lower radiative state lifetime and also a measure of injection efficiency.[19,20] The small differential resistance drop in design 2 is an indication of poorer injection efficiency, compared to the first two designs. At the end of the tunneling resonance, onset of high differential resistance is more gradual in design 2. The high differential resistance region is also narrower and the differential resistance is relatively low. These are all indications of degraded selectivity of injection and extraction. EMC simulations show that the oscillator strength of design 2 increases a lot, compared to the reference structure that leads to superior performance at higher temperatures. However, these results could be inaccurate due to the limitations of our EMC simulations, which do not consider leakage to continuum and aperiodicity of the biased QCL stages (i.e., domain formation). Another reason for the discrepancy between EMC simulations and experiment may be parameter uncertainties (percentage of donors that are ionized, interface roughness parameters) and the fact that some effects such as higher-order scattering events and tunneling are not included in the simulations. Further refinement of EMC simulation parameters is needed to improve its predictive power for the step barrier design.

Design 1 shows the more promising performance. In contrast to design 2, T_{max} of design 1 is comparable to the reference and the I-V curves are very similar to the reference except the difference in current. Fig. 5 plots the threshold current density versus temperature. The threshold current density of design 1 is almost constantly 25% higher than that of the reference. Since the sheet doping density per QCL period in all structures was the same and the injection/extraction barrier thickness and composition is identical for design 1 and the reference structure, the higher current density may be attributed to parasitic channels due to the reduced barrier height in the active region resulting in an increased coupling of the states.

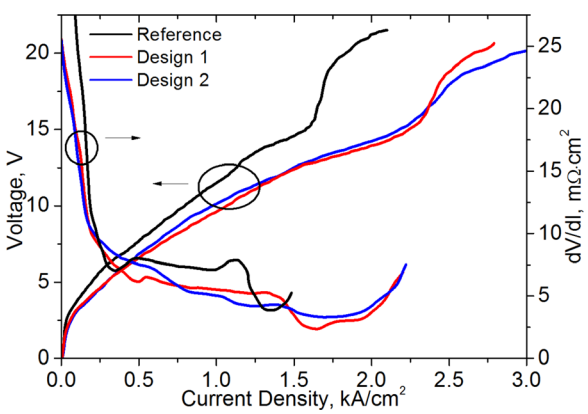

FIG. 4. Current density-voltage (I-V) characteristics and differential resistance versus current density (dV/dI-I) data for the three designs tested at 150 K.

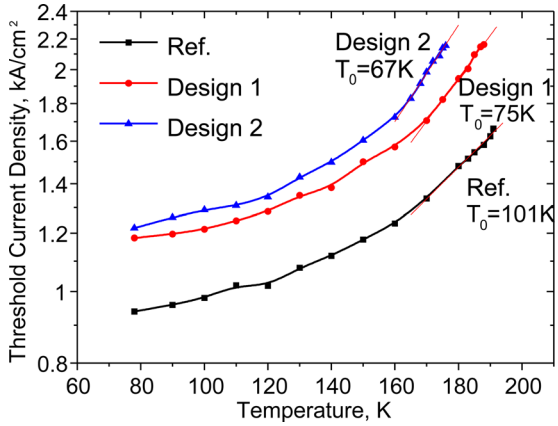

FIG. 5. Threshold current density vs. temperature for the three designs tested.

V. CONCLUSION

To summarize, we have performed an experimental study on THz QCLs with variable barrier heights. The devices did not achieve maximum operating temperatures superior to that of the reference record structure; however, the maximum operating temperature of design 1 was very similar to that of the reference laser. The results indicate that variation of aluminum fraction in barriers during device growth does not result in significant laser performance deterioration and using barriers with variable aluminum fractions in the THz QCL active region is a viable approach to enhance the design space for THz QCLs.

ACKNOWLEDGMENTS

The University of Texas group acknowledges support from the NSF Grant No. ECCS-1150449 and DARPA Grant No. 66001-12-14241.

[1]R. Köhler, A. Tredicucci, F. Beltram, H. E. Beere, E. H. Linfield, A G. Davies, D. A. Ritchie, R. C. Iotti, and F. Rossi, Nature **417**(6885), 156 (2002).
[2]S. Fathololoumi, E. Dupont, C. W. I. Chan, Z. R. Wasilewski, S. R. Laframboise, D. Ban, A. Matyas, C. Jirauschek, Q. Hu, and H. C. Liu, Opt. Express **20**(4), 3866 (2012).
[3]H. Luo, S. R. Laframboise, Z. R. Wasilewski, G. C. Aers, H. C. Liu, and J. C. Cao, Appl. Phys. Lett. **90**(4), 041112 (2007).
[4]B. S. Williams, H. Callebaut, S. Kumar, Q. Hu, and J. L. Reno, Appl. Phys. Lett. **82**(7), 1015 (2003).
[5]M. A. Belkin, J. A. Fan, S. Hormoz, F. Capasso, S. P. Khanna, M. Lachab, A. G. Davies, and E. H. Linfield, Opt. Express **16**(5), 3242 (2008).
[6]S. Kumar, C. W. I. Chan, Q. Hu, and J. L. Reno, Nat. Phys. **7**(2), 166 (2011).
[7]B. S. Williams, Nat. Photonics **1**(9), 517 (2007).
[8]M. A. Belkin, Q. J. Wang, C. Pflugl, A. Belyanin, S. P. Khanna, A. G. Davies, E. H. Linfield, and F. Capasso, IEEE J. Sel. Top. Quantum Electron. **15**(3), 952 (2009).
[9]Y. Chassagneux, Q. J. Wang, S. P. Khanna, E. Strupiechonski, J. Coudevylle, E. H. Linfield, A. G. Davies, F. Capasso, M. A. Belkin, and R. Colombelli, IEEE Trans. THz Sci. Technol. **2**(1), 83 (2012).
[10]S. Kumar, Q. Hu, and J. L. Reno, Appl. Phys. Lett. **94**(13), 131105 (2009).
[11]A. Matyas, M. A. Belkin, P. Lugli, and C. Jirauschek, Appl. Phys. Lett. **96**(20), 201110 (2010).

[12]S. Fathololoumi, E. Dupont, Z. R. Wasilewski, C. W. I. Chan, S. G. Razavipour, S. R. Laframboise, S. Huang, Q. Hu, D. Ban, and H. C. Liu, J. Appl. Phys. **113**(11), 113109 (2013).
[13]A. Matyas, R. Chashmahcharagh, I. Kovacs, P. Lugli, K. Vijayraghavan, M. A. Belkin, and C. Jirauschek, J. Appl. Phys. **111**(10), 103106 (2012).
[14]G. Scalari, M. I. Amanti, M. Fischer, R. Terazzi, C. Walther, M. Beck, and J. Faist, Appl. Phys. Lett. **94**(4), 041114 (2009).
[15]C. Jirauschek and P. Lugli, Phys. Status Solidi C **5**, 221 (2008).
[16]W. Freeman and G. Karunasiri, Phys. Rev. B **85**(19), 195326 (2012).
[17]Z. R. Wasilewski "MBE growth of THz quantum cascade lasers," in *Molecular Beam Epitaxy: From Research to Mass Production*, edited by M. Henini (Elsevier, 2012).
[18]M. P. Patkar, T. P. Chin, J. M. Woodall, M. S. Lundstrom, and M. R. Melloch, Appl. Phys. Lett. **66**(11), 1412 (1995).
[19]B. S. Williams, S. Kumar, Q. Hu, and J. L. Reno, Opt. Express **13**(9), 3331 (2005).
[20]C. Sirtori, F. Capasso, J. Faist, A. L. Hutchinson, D. L. Sivco, and A. Y. Cho, IEEE J. Quantum Electron. **34**(9), 1722 (1998).